Article ID: 1001-3555(2018)05-0461-10

Graphitic Carbon Nitride (g-C_3N_4) Photocatalyzed Degradation MO using EDTA as Efficient Accelerating Agent

TANG Dan, YIN Meng-yun, SONG Xue-ping, ZHOU Li-mei, ZHOU Ya-fen*

(*Chemical Synthesis and Pollution Control Key Laboratory of Sichuan Province, China West Normal University, Nanchong* 637000, *Sichuan, China*)

Abstract: The enhancement of g-C_3N_4 photocatalytic degradation of methyl orange (MO) via ethylenediaminetetraacetic acid (EDTA) addition was investigated under light irradiation. The effects of H^+ and carboxylate anions on the MO degradation were investigated in this reaction. An investigation by UV-vis diffuse reflectance spectroscopy (DRS) reveals that the addition of EDTA has not changed the electronic structure and photoelectric property of g-C_3N_4. It was considered that the addition of EDTA trapped the holes (h^+) and promoted the separation rate of the e^-/h^+ pairs, resulting in an increase in photodegradation activity. It is verified that $\cdot O_2^-$ species are the major oxide species during photocatalytic degradation process. Therefore, a plausible mechanism that EDTA promotes photodegradation of MO by g-C_3N_4 is proposed. This work provides a new approach for a better catalytic performance of g-C_3N_4 on treatment of organic contaminants in aqueous system.

Key words: g-C_3N_4; ethylenediaminetetraacetic acid; methyl orange; photocatalysis; photodegradation

CLC number: O643.36 **Document code**: A

Increasing water pollution is one of the greatest challenges to the environment. Industries based on textiles, leather, food and cosmetics use large amount of dyes, and the organic pollutants from these industries is a major environmental anxiety. Methyl orange (MO) is one of the main sources of water pollution, which is an intensely colored compound used in dyeing and printing textiles. Therefore, seeking efficient, greenand safe purification technologies and materials which can effectively remove organic pollutants from wastewater are of great significance to environmental protection. Semiconductor materials have great potential in environmental and energetic applications, because they can eject an electron from the valence band to the conduction band under irradiation at the proper wavelength, where it is mobile and can be used for photocatalytic degradation reactions[1-3].

Since the early report of graphitic carbon nitride (g-C_3N_4) photocatalysts in the H_2 evolution in 2009, the metal-free conjugated polymeric semiconductor has gained considerable interdisciplinary interest[4]. Owing to its visible light response, high chemical and thermal stability, a relatively narrow band gap of 2.7 eV, reasonable cost, "earth-abundant" nature, flexible super molecular networks and environmentally benign characteristics, g-C_3N_4 has been considered as the next generation photocatalyst in the research communities[5-8]. However, the intrinsic drawbacks of graphitic carbon nitride, especially the high recombination of photogenerated charge carriers, the limited active sites, low specific surface area and the serious aggregation during the photocatalytic process, seriously restrict the catalytic vigor[9-10]. Thus, to promote the separation of photogenerated electrons (e^-) and holes (h^+) pairs would be a key factor for the photocatalytic degradation of organic contaminants[11]. Many studies have been devoted to improve the separation rate of charge carriers by modified g-C_3N_4 using metal and non-metal heteroa-

Received date: 2018-07-29; **Revised date**: 2018-08-20.

Foundation: The authors are grateful for financial support from the Key Project of the Education Department of Sichuan Province (18ZA0474) and the Project of Talents Research Fund of China West Normal University (17YC040).

First author: Tang Dan, female, born in 1995, master.

Corresponding author: Zhou Yafen, female, born in 1971, doctor, Tel: +86-817-2568081; E-mail: cwnuzyf@163.com.

tom[12-13], fabricating heterojunctions with other semiconductors[14], and nanostructure modulations[15-16], etc. However, most of these methods are complicated, time consuming, and unfriendly to the environment. Therefore, an easy way to increase the activity of carbon nitride is urgently needed. Liu et al. reported that persulfate (PS) captured photogenerated e^- and then reduced O_2 into $\cdot O_2^-$, thus boosted the separation of photogenerated e^-/h^+ pairs and led to the increase of the g-C_3N_4 photocayalytic performance[17]. So, it is a simple and effective way to improve the photocatalytic performance of g-C_3N_4 by adding an e^- or h^+ trapping agent to promote the separation of photogenerated e^-/h^+ pairs.

We all know that EDTA-2Na is commonly used as an h^+-trapping agent in capture experiments. However, an interesting experimental phenomenon that the photocatalytic degradation rate was remarkably increased in the presence of EDTA-2Na has been observed. This phenomenon has also been found in other literatures[18-21]. What's more, we found that EDTA promoted the photocatalytic degradation of MO by g-C_3N_4 at a higher rate than EDTA-2Na. A possible reaction mechanism is proposed by the capture experiments. These results indicated that acidic conditions favor the degradation of MO, h^+ is trapped and the separation of photogenerated e^-/h^+ pairs is promoted when EDTA is added. So, the photocatalytic activity of g-C_3N_4 remarkably improved. This work could inspire an idea of adding some kind of agents which could react with e^- or h^+ to reduce the recombination of photo-generated carriers, then, achieved a highly efficient photocatalytic reaction.

1 Materials and methods

1.1 Synthesis of g-C_3N_4

The g-C_3N_4 sample was prepared by a previously reported thermal polymerization method[22]. The g-C_3N_4 powder was synthesized typically by heating 5 g of melamine in a semi-closed quartz crucible with a cover in a nitrogen atmosphere. The heating program was as follows: heating to 550 ℃ at the rate of 5 ℃/min and holding for 4 h, then naturally cooling to room temperature. The product was collected and ground into powder.

1.2 Catalyst characterization

Fourier transform infrared (FTIR) spectroscopy was gained by a Themo Scientific Nicolet-6700 FTIR spectrophotometer. X-ray diffraction (XRD) patterns were recorded by a Rigaku Dmax/Ultima IV diffractometer with monochrommatized Cu kα radiation (k = 1.5418 Å). Scanning electron microscopy (SEM) was taken with a JEOL JSM-6510LV scanning electron microscopy. And UV-vis diffuse reflectance spectra (DRS) was recorded on a Shimazu UV-3600 spectrophotometer equipped with diffuse reflectance accessories, using $BaSO_4$ as the reference sample. X-Ray photoelectron spectroscopy (XPS) measurements were carried outusing an ESCALAB 250 Xi with a high-performance Al monochromatic source (hv = 1486.6 eV, 150 W). All binding energies were referenced to the C 1s peak at 284.8 eV of surface adventitious carbon, and the elemental compositions were determined from peak area ratios after correction for the sensitivity factor for each element. Brunauer-Emmett-Teller (BET) surface area measurements were conducted using the N_2 adsorption-desorption isotherms obtained at 77 K using Quantachrome Instruments version 3.0.

1.3 Photocatalytic activity

The photocatalytic activities of the prepared sample were assessed by the photodegradation of MO under the UV-visible light irradiation by using a 70 W metal halide at ambient temperature in air with magnetic stirring[23-25]. In a typical experiment, 25 mg of g-C_3N_4 and 1 mmol/L Ethylenediaminetetraacetic acid (EDTA) were dispersed into 50 mL MO aqueous solution (10 mg/L) at room temperature. Before the light irradiation, the suspension was firstly sonicated for 10 min and then magnetically stirred for 20 min in the dark to obtain an adsorption-desorption equilibrium. Then the light was turned on and a 3 mL sample was taken out at certain time intervals from the reaction system and centrifuged to remove the photocatalyst powders for analysis. The concentration of the target pollutant was analyzed by using a Shimadzu UV-2550 UV-vis spectrophotometer. The relative concentration (C/C_0) of the

MO solution was calculated at 463 nm, in which C_0 and C are the concentrations of MO at the beginning of light irradiation and at time t respectively.

1.4 Active species detection

Radical capturing experiments were conducted to identify the possible photocatalytic reaction mechanism of this reaction system. The detection process was similar to the photodegradation experimental process. Three radical scavengers, isopropanol (IPA) as hydroxyl radical (·OH) scavenger, ethylenediamineteraacetic acid disodium salt (EDTA-2Na) as h^+ radical scavenger and *p*-benzoquinone (BQ) as superoxide radical ($\cdot O_2^-$) scavenger, were selected to investigate the role of radicals in the photocatalytic degradation of MO[24-25].

2 Results and discussions

2.1 Structural characteristics

The as-prepared g-C_3N_4 was characterized by a series of methods (XRD, FTIR and SEM). Fig. 1a shows the XRD pattern of as-prepared g-C_3N_4. The catalyst exhibits two peaks at 12.8° and 27.4°, corresponding to (100) and (002) crystal planes of g-C_3N_4. The characteristic peak at 27.4° corresponds to the interlayer stacking reflection of conjugated aromatic systems. The weak peak at 12.8° can be attributed to in-plane repeating units of continuous heptazine framework. The chemical structures of the photocatalysts were analyzed by FTIR spectrum, as shown in Fig.1b. Three strong absorption peaks at 3650 ~ 3300 cm^{-1}, 1240 ~ 1650 cm^{-1} and 810 cm^{-1} present in the sample. The broad peak at 3650 ~ 3300 cm^{-1} is ascribed to the stretching vibration of N − H and the stretching vibration of O−H of the surface adsorbed water molecules. The peaks in the range of 1240 ~ 1650 cm^{-1} belongs to the stretching vibrations of tri-s-trizaine skeleton ring, and the bending mode of trizaine units at 810 cm^{-1}. The morphology and microstructure of the g-C_3N_4 was characterized by SEM. As can be seen in Fig.1c, the g-C_3N_4 composes a large number of irregular particles. As shown in Fig.1, the results are consistent well with reported in the literatures[26-31].

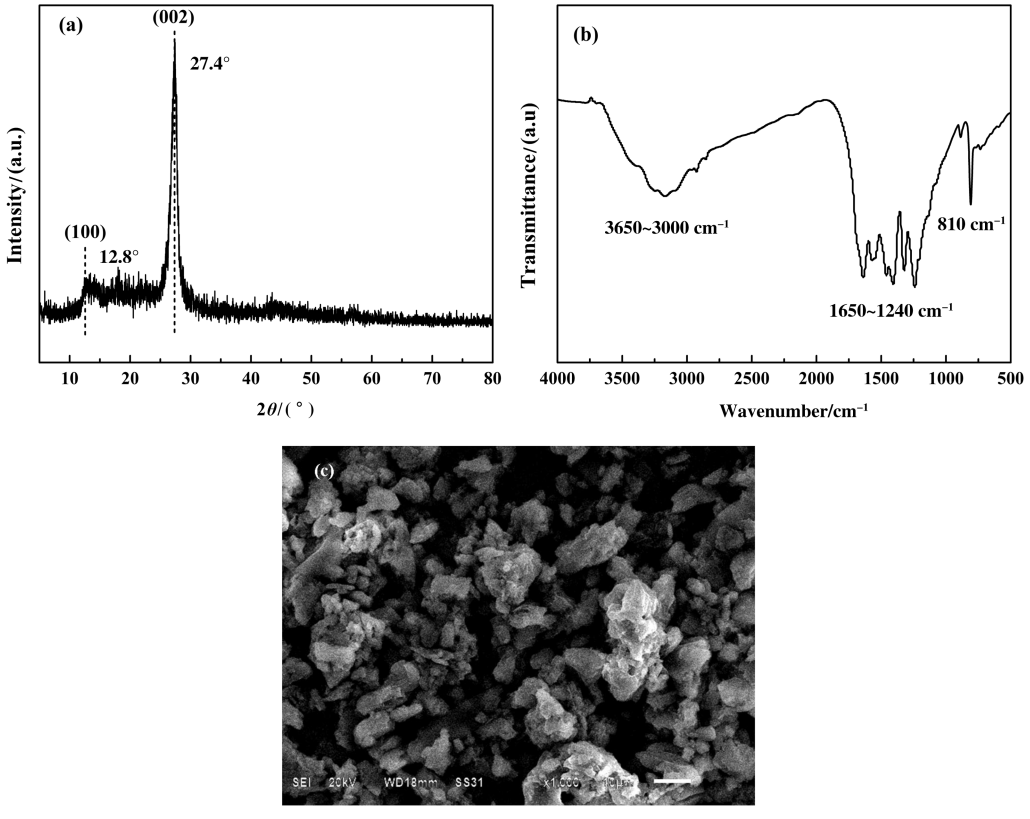

Fig.1 (a) The XRD pattern, (b) the FTIR spectrum and (c) the SEM image of g-C_3N_4

2.2 Effect of EDTA on degradation of MO

Fig.2a illustrates the influence of the addition of EDTA on the degradation of MO. As shown in Fig.2a, negligible removal of MO was found in the presence of g-C_3N_4(CN) after 20 min of irradiation, but 97.59% MO was degraded in the addition of EDTA under the same condition. This result indicated that the addition of EDTA greatly promotes the photocatalytic degradation of MO.

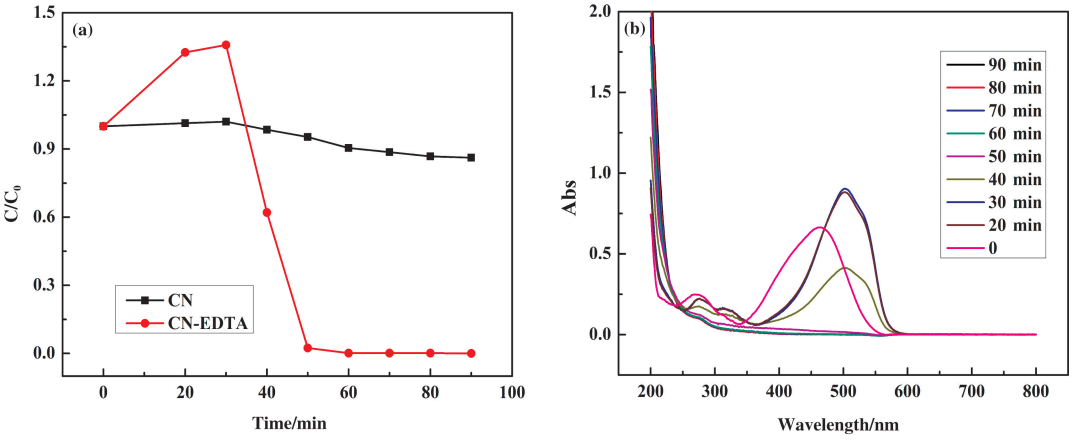

Fig.2 (a) Photocatalytic degradation rate of MO and (b) spectral changes during photocatalytic degradation under light irradiation

As shown in Fig.2b, due to the addition of EDTA, the maximum absorption wavelength of MO is red-shifted from 463 to 501 nm, and the intensity of the absorption peak increased before the light irradiation. For MO, it has quinoid and azo structures under acidic and basic conditions, respectively. The chemical structure of MO changes following the equation in Fig.3[32]. The addition of EDTA increased the acidity of the MO solution , made the structure of MO changed from azo to quinoid, and the color of the solution changed from yellow to orange-red. Therefore, the maximum absorption wavelength of MO is red-shifted and the peak intensity is changed in the UV-Vis absorption spectrum. So, the relative concentration (C/C_0) of the MO solution is calculated at 463 and 510 nm, in which C_0 and C are the concentrations of MO at the beginning of light irradiation and at time t respectively. From the calculation results, the value of C/C_0 is greater than 1 during the dark.

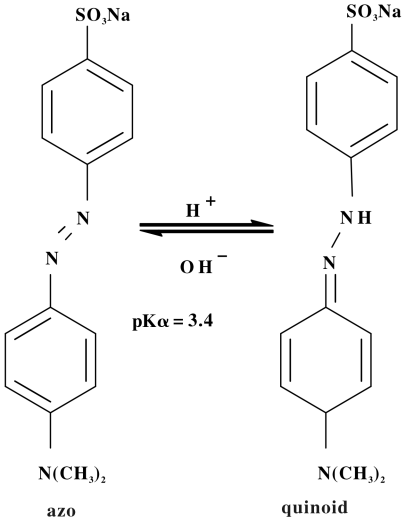

Fig.3 The chemical structure changes of MO

2.3 Mechanism for the photocatalysis

Herein, a series of tests were designed to probe the photocatalytic degradation process. Firstly, to identify the main active species in the photocatalytic degradation process, the trapping experiments by adding various scavengers were conducted. As we all know, BQ can scavenge $\cdot O_2^-$ from the reduction reaction of O_2 by photoexcited electrons on conduction band (CB), IPA can quench $\cdot$OH which is generated by the oxidation of water by h^+ and EDTA-2Na can trap photogenerated h^+ on valence band (VB). From Fig.4a, the photocatalytic activity of g-C_3N_4 is seriously suppressed by the addition of BQ, indicating that $\cdot O_2^-$ is the main active specie in the photocatalytic reaction. Negligible effect of IPA on the degradation of MO is observed, revealed that $\cdot$OH radical is not the domina-

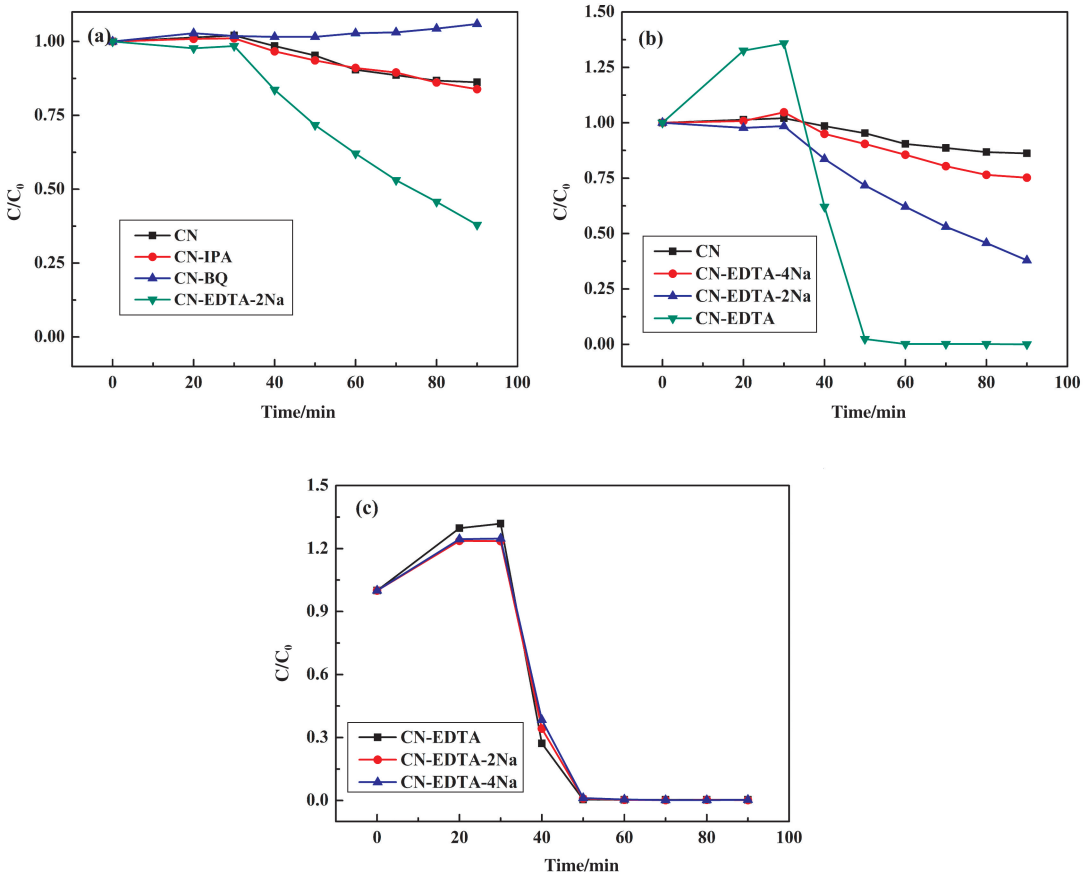

Fig.4 (a) Photocatalytic activities of g-C_3N_4 for the degradation of MO in the presence of different scavengers (1 mmol/L); (b) Photocatalytic activities in the addition of EDTA, EDTA-2Na and EDTA-4Na in the same concentration, respectively and (c) the changes in the same pH.

ting active species for MO photodegradation. However, in the presence of EDTA-2Na, the photocatalytic degradation was improved to a certain extent. This interesting phenomenon inspired us to further study.

As we known, EDTA, EDTA-2Na and EDTA-4Na all contain four carboxyl groups, but their aqueous solutions are different in acidity and basicity. So, under the same experimental conditions, the effects of EDTA, EDTA-2Na and EDTA-4Na on the photocatalytic degradation of MO over g-C_3N_4 were compared with the additives were all at the same concentration (1 mmol/L). The pH values of EDTA, EDTA-2Na and EDTA-4Na solutions are 2.35, 4.31, and 9.24, respectively. The experimental results are shown in Fig. 4b. The photodegradation activities of MO were improved after adding the three reagents respectively, but the effect of EDTA on the promotion was the most obvious that led the MO almost completely degrade after 20 min of light irradiation. EDTA-4Na also had a certain increase of the degradation, but it was not as good as EDTA and EDTA-2Na. MO degraded only 24.8% with EDTA-4Na addition, while EDTA-2Na can reach 62.08% after only 1 hour of light irradiation. The main differences of these three substances are the acidity, it is obvious that the H^+ concentration of EDTA aqueous solution is the largest and the smallest is EDTA-4Na. Under acidic condition, MO dye had higher photocatalytic degradation efficiency based on these experimental results. So, we may infer that its quinoid structure is more prone to photocatalytic degradation than the azo structure.

The pH of the EDTA, EDTA-2Na, and EDTA-4Na systems was adjusted to be the same and degraded under illumination (pH =2.35). As shown in Fig.4c,

the changes in these three systems are almost negligible, further demonstrated the addition of EDTA, EDTA-2Na and EDTA-4Na mainly changed the acidity of the reaction solution.

To verify the influence of carboxylate anions on the degradation of MO by EDTA, the photocatalytic performance of g-C_3N_4 photocatalyzed degradation MO was compared by using HCl and EDTA as additives in the same pH (3.03), respectively. As shown in Fig.5a, after 20 min of light irradiation, 33% and 98%

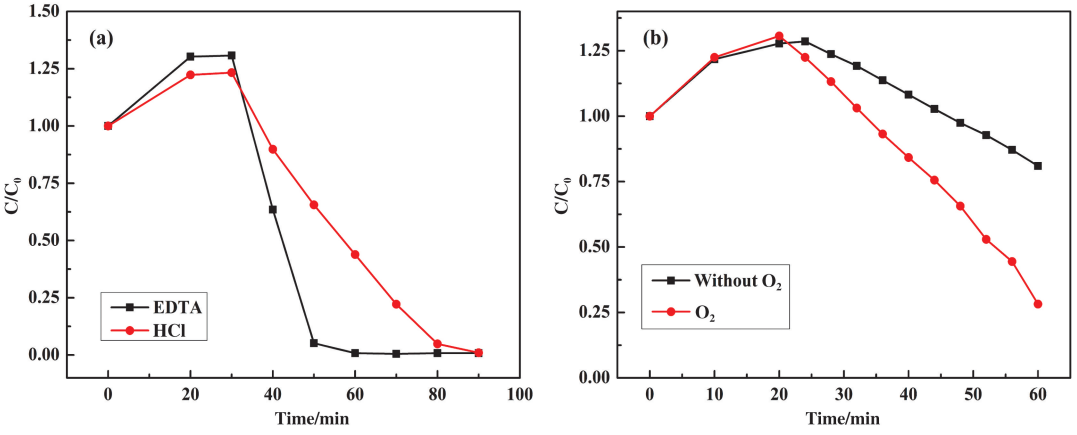

Fig.5 (a) The comparison of photocatalytic activity of the presence of HCl and EDTA for degradation of MO. (b) The comparison of photocatalytic activity of the presence of O_2 and without O_2 for degradation of MO.

of MO is degraded in the presence of HCl and EDTA, respectively, EDTA have a superior efficiency than HCl. The effect of EDTA is greater than that of HCl under the same pH, indicating that the H^+ is not the only factor for the degradation of MO, whereas carboxyl group also plays an important role. According to the 'photo-Kolbe' reaction[33], carboxylate anions can react with h^+ to generate organic radicals after removal of CO_2. Photogenerated h^+ are constantly accepted by carboxylate anions in EDTA, reducing the recombination of e^- and h^+, resulting in an increase in the amount of $\cdot O_2^-$ which is formed by the reduction reaction of O_2 by photoexcited e^-. Finally, MO is degraded by $\cdot O_2^-$.

According to the result of Fig. 4a, $\cdot O_2^-$ is the main active species in the photocatalytic degradation process. EDTA as an efficient h^+ accepter is conducive to the charge separation and lowering the recombination rate of photogenerated e^-/h^+ pairs then bring about higher photocatalytic degradation rate. To further verify the role of $\cdot O_2^-$, formed by the reduction reaction of O_2 by photoexcited e^-, the photocatalytic degradation of MO were compared with and without O_2[34]. As shown in Fig.5b, it can be clearly observed that the photodegradation reaction is rather weaker without O_2. When the air was isolated the formation of $\cdot O_2^-$ was reduced, therefore, the rate of photodegradation decreased.

To identify the change of electronic structure and photoelectric property of g-C_3N_4 with the addition of EDTA, UV-vis diffuse reflectance spectroscopy (DRS) (Fig.6a) were used to characterize the g-C_3N_4 and the mixture of g-C_3N_4 and EDTA after sonicated and stirred (CN-EDTA). As shown in Fig.6a, there is no obvious change in the absorption edge and derived electronic band gaps. So, the addition of EDTA has not changed the electronic structure and photoelectric property of g-C_3N_4. The Brunauer-Emmett-Teller (BET) surface areas of CN and CN-EDTA were measured by N_2 adsorption-desorption measurements at 77.4 K. As shown in Fig.6b, the BET surface area of CN-EDTA is a little larger than CN. Thus, we suspect that EDTA promotes g-C_3N_4 degradation of MO may also be due to an increase of CN surface area.

To further research the CB and VB of g-C_3N_4, the valence band X-ray photoelectron spectroscopy (VB XPS) was tested. From Fig.7, it can be seen that the

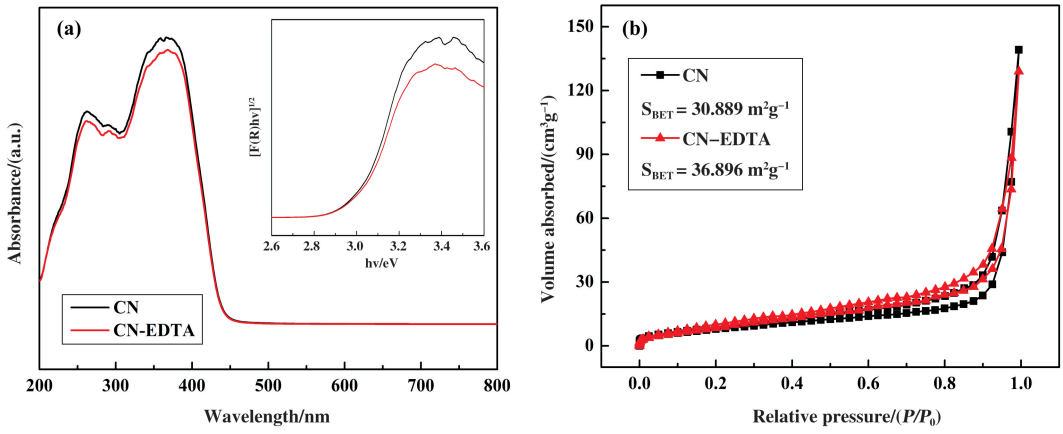

Fig.6 (a) UV-vis diffuse reflectance of spectra; (b) The N_2 adsorption-desorption isotherms

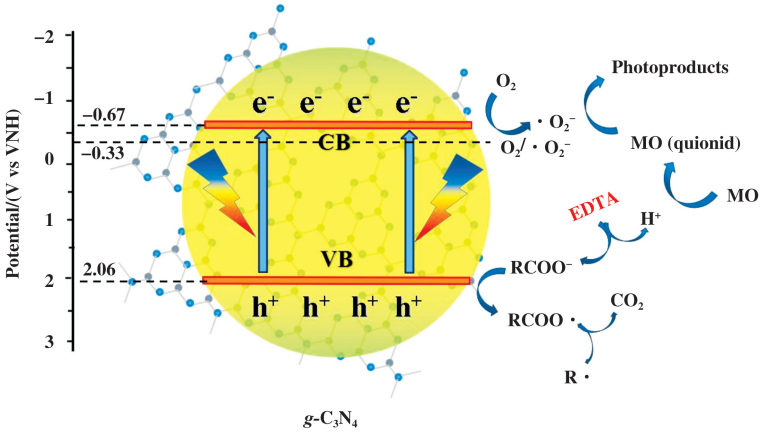

Fig.7 Schematic illustration for the photocatalytic degradation of MO dye over g-C_3N_4 in the addition of EDTA

VB potential of CN is 2.06 eV (vs. NHE). Combined with the UV-vis DRS result, the CB potential of CN is −0.67 eV (vs. NHE). From Fig.7, we see that the CB edge potential of CN is more negative than the standard redox potential $O_2/\cdot O_2^-$ (−0.33 V vs. NHE) to reduce the molecular oxygen to yield $\cdot O_2^-$. But the VB potential of CN is small difference with the standard redox potential of $OH^-/\cdot OH$ (+1.99 V vs. NHE)[35]. Consequently, we might infer the h^+ cannot efficiently oxidize OH^- to generate $\cdot OH$ radicals. The above conclusions are consistent with the results of the trapping experiments.

Based on the above results, a plausible mechanism of EDTA promoted photodegradation of MO by g-C_3N_4 was proposed:

$$g\text{-}C_3N_4 + h\nu \longrightarrow g\text{-}C_3N_4\text{-}h^+ + g\text{-}C_3N_4\text{-}e^- \quad (1)$$

$$g\text{-}C_3N_4\text{-}e^- + O_2 \longrightarrow \cdot O_2^- + g\text{-}C_3N_4 \quad (2)$$

$$MO + EDTA \longrightarrow MO\ (quinoid) + RCOO^- \quad (3)$$

$$RCOO^- + g\text{-}C_3N_4\text{-}h^+ \longrightarrow RCOO\cdot + g\text{-}C_3N_4 \quad (4)$$

$$RCOO\cdot \longrightarrow R\cdot + CO_2 \quad (5)$$

$$MO\ (quinoid) + \cdot O_2^- \longrightarrow Photoproducts \quad (6)$$

As depicted in Fig.7, the photogenerated e^- and h^+ are produced in the conduction band (CB) and valence band (VB) of g-C_3N_4 under irradiation (Eq.1). The photogenerated e^- can induce the adsorbed O_2 into $\cdot O_2^-$ (Eq.2) because of its sufficient reductive ability. Meanwhile, the addition of EDTA makes the aqueous solution acidic and the structure of MO at this time is quinoid (Eq.3). Carboxylate anions capture photogenerated h^+ which inhibits the recombination of photogenerated e^- and h^+ pairs and generate organic radicals after removal of CO_2 (Eq.4 and 5). EDTA promotes the

separation of e^- and h^+ pairs, increasing the amount of $\cdot O_2^-$ which could oxidize MO (quinoid) to products (Eq.6). Finally, g-C_3N_4 photocatalytic degradation of MO greatly increased.

2.4 Effect of EDTA on degradation of other pollutant

To confirm the universality of the method, we have studied the photocatalytic degradation of rhodamine B (RhB). Under the same conditions, this reaction system used 25 mg g-C_3N_4, 1 mmol/L Ethylenediaminetetraacetic acid (EDTA), 50 mL RhB aqueous solution (10 mg/L), and the relative concentration (C/C_0) of the RhB solution was calculated at 554 nm. As shown in Fig.8, 99% RhB is degraded in the addition of EDTA after 20 min of irradiation, while only 16.37% RhB is degraded in the presence of g-C_3N_4. The result also verified the excellent ability of the addition of EDTA to remove organic pollutants in water.

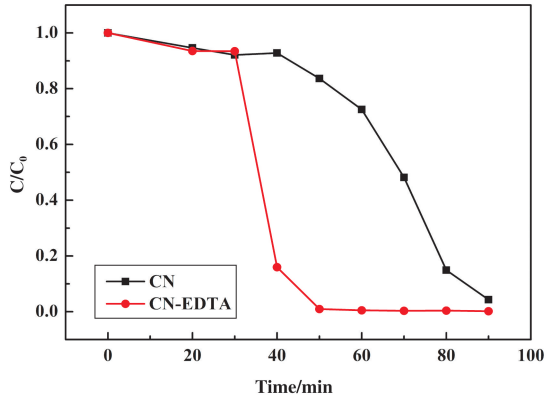

Fig.8 Photocatalytic degradation of RhB

3 Conclusions

In this work, we demonstrated an efficient approach to improve the photocatalytic activity of g-C_3N_4 by adding EDTA. According to the experimental results, EDTA trapped the h^+ and effectively promoted the separation rate of the e^-/h^+ pairs, which is the main reason for the raised photocatalytic activity of g-C_3N_4. What's more, the addition of EDTA has not changed the electronic structure and photoelectric property of g-C_3N_4. The trapping experiments verified that $\cdot O_2^-$ is the major oxide specie for the photocatalytic degradation of MO, then, the plausible mechanism was proposed. This work offers a new promising route for the rapid degradation of organic pollutants by adding some kind of agents to inhibit the recombination of e^-/h^+ pairs of the photocatalysts.

References:

[1] a. Park T J, Pawar R C, Kang S, *et al.* Ultra-thin coating of g-C_3N_4 on an aligned ZnO nanorod film for rapid charge separation and improved photodegradation performance[J]. *RSC Adv*, 2016, **6**(92): 89944-89952.
b. Tian Chang-shui(田长水), Liu Ya-ting(刘雅婷), Sheng Wen-long(盛文龙), *et al.* Preparation of TiO_2 nanofibers templated with mesoporous SiO_2 spheres and photocatalytic synthesis of ammonia(介孔 SiO_2球为模板制备 TiO_2纳米纤维及光催化合成氨)[J]. *J Mol Catal (China)*(分子催化), 2016, **30**(6): 566-574.
c. Yi Ru(意 如), Bai Sagala(萨嘎拉), Bao Zhaorigetu(照日格图). Preparation of Pd/MCM-41 and its photocatalytic performance for benzene hydroxylation (Pd/MCM-41 催化剂的制备及其光催化苯羟基化的研究)[J]. *J Mol Catal(China)*(分子催化), 2016, **30**(6): 583-593.

[2] a. Meng Z D, Zhu L, Choi J G, *et al.* Effect of Pt treated fullerene/TiO_2 on the photocatalytic degradation of MO under visible light [J]. *J Mater Chem*, 2011, **21**(21): 7596-7603.
b. Lu Gong-xuan(吕功煊), Zhen Wen-long(甄文龙). Formation of helium-3 and helium-4 during photocatalytic hydrogen generation over cadmium sulfideunder visible light irradiation(半导体 CdS 悬浮体系中可见光催化产氢同时生成氦-3 和氦-4)[J]. *J Mol Catal(China)*(分子催化), 2017, **31**(4): 299-304.

[3] a. Wu Yu-qi(吴玉琪), Jin Zhi-liang(靳治良), Li Yue-xiang(李越湘), *et al.* Recent development of semiconductor photocatalysts for hydrogen generation(半导体光催化剂制氢研究新进展)[J]. *J Mol Catal(China)*(分子催化), 2010, **24**(2): 171-194.
b. Lu Gong-xuan(吕功煊), Zhang Wen-yan(张文妍). Photocatalytic hydrogen evolution and induced transmutation of potassium to calcium via low-energy nuclear reaction(LENR) driven by visible light (可见光驱动的光催化产氢同时诱导低能核反应嬗变钾为钙)[J]. *J Mol Catal(China)*(分子催化), 2017, **31**(5): 401-410.

[4] a. Cao S W, Low J X, Yu J G, *et al.* Polymeric photocatalysts based on graphitic carbon nitride [J]. *Adv Mater*, 2015, **27**(13): 2150-2176.
b. Sarenqiqige(萨仁其其格), Bai Sagala(萨嘎拉), Jia

Mei-lin(贾美林), *et al.* Photocatalytic degradation of acetic acid in wastewater by TiO_2/Fe-Hangjin 2 # catalyst (TiO_2/Fe-杭锦 2 # 土催化剂光催化降解废水中乙酸的研究)[J]. *J Mol Catal*(*China*)(分子催化), 2017, **31**(6): 523-533.

[5] Wang Y, Wang X C, Antonietti M. Polymeric graphitic carbon nitride as a heterogeneous organocatalyst: From photochemistry to multipurpose catalysis to sustainable chemistry [J]. *Angew Chem Int Ed*, 2012, **51**(1): 68-89.

[6] Zheng Y, Lin L, Wang B, *et al.* Graphitic carbon nitride polymers toward sustainable photoredox catalysis [J]. *Angew Chem Int Ed*, 2015, **54**(44): 12868-12884.

[7] Wang X C, Maeda K, Thomas A K, *et al.* A metal-free polymeric photocatalyst for hydrogen production from water under visible light [J]. *Nat Mater*, 2009, **8**(1): 76-80.

[8] Ma Lin(马 琳), Kang Xiao-xue(康晓雪), Hu Shao-zheng(胡绍争), *et al.* Preparation of Fe-P Co-doped graphitic carbon nitride with enbonced visible-light photocatalytic activity(Fe-P 共掺杂石墨相氮化碳催化剂可见光下催化性能研究)[J]. *J Mol Catal*(*China*)(分子催化), 2015, **29**(4): 359-368.

[9] Liang Q H, Li Z, Huang Z H, *et al.* Holey graphitic carbon nitride nanosheets with carbon vacancies for highly improved photocatalytic hydrogen production [J]. *Adv Funct. Mater*, 2015, **25**(44): 6885-6892.

[10] Liu J, Wang H Q, Antonietti M. Graphitic carbon nitride "reloaded": Emerging applications beyond (photo) catalysis [J]. *Chem Soc Rev*, 2016, **45**(8): 2308-2326.

[11] Ye C, Wang X Z, Li J X, *et al.* Protonated graphitic carbon nitride with surface attached molecule as hole relay for efficient photocatalytic O_2 evolution [J]. *ACS Catal*, 2016, **6**(12): 8336-8341.

[12] Jiang J, Cao S W, Hu C L, *et al.* A comparison study of alkali metal-doped g-C_3N_4 for visible-light photocatalytic hydrogen evolution [J]. *Chin J Catal*, 2017, **38**(12): 1981-1989.

[13] Cao S W, Huang Q, Zhu B C, *et al.* Trace-level phosphorus and sodium co-doping of g-C_3N_4 for enhanced photocatalytic H_2 production [J]. *J Power Sour*, 2017, **351**: 151-159.

[14] Liu H H, Chen D L, Wang Z Q, *et al.* Microwave-assisted molten-salt rapid synthesis of isotype triazine-/heptazine based g-C_3N_4 heterojunctions with highly enhanced photocatalytic hydrogen evolution performance [J]. *Appl Catal B*: *Environ*, 2017, **203**: 300-313.

[15] Zheng D D, Pang C Y, Liu Y X, *et al.* Shell-engineering of hollow g-C_3N_4 nanospheres by copolymerization for photocatalytic hydrogen evolution [J]. *Chem Commun*, 2015, **51**: 9706-9709.

[16] Wang Z Y, Guan W, Sun Y J, *et al.* Water-Assisted production of honeycomb-Like g-C_3N_4 with ultralong carrier lifetime and outstanding photocatalytic activity [J]. *Nanoscale*, 2015, **7**: 2471-2479.

[17] Liu B C, Qiao M, Wang Y B, *et al.* Persulfate enhanced photocatalytic degradation of bisphenol A by g-C_3N_4 nanosheets under visible light irradiation [J]. *Chemosphere*. 2017, **189**: 115-122.

[18] Hu S Z, L Ma, You J G, *et al.* A simple and efficient method to prepare a phosphorus modified g-C_3N_4 visible light photocatalyst[J]. *RSC Adv*, 2014, **4**(41): 21657-21663.

[19] Shi W L, Guo F, Chen J B, *et al.* Hydrothermal synthesis of $InVO_4$/Graphitic carbon nitride heterojunctions and excellent visible-light-driven photocatalytic performance for rhodamine B [J]. *J Alloys Compd*, 2014, **612**: 143-148.

[20] Zhang J, Hu S Z, Wang Y J. A convenient method to prepare a novel alkali metal sodium doped carbon nitride photocatalyst with a tunable band structure [J]. *RSC Adv*, 2014, **4**(108): 62912-62919.

[21] Xu K, Feng J. Superior photocatalytic performance of $LaFeO_3$/g-C_3N_4 heterojunction nanocomposites under visible light irradiation [J]. *RSC Adv*, 2017, **7**(72): 45369-45376.

[22] Ho W K, Zhang Z Z, Xu M K, *et al.* Enhanced visible-light-driven photocatalytic removal of NO: Effect on layer distortion on g-C_3N_4 by H_2 heating [J]. *Appl Catal B*: *Environ*, 2015, **179**: 106-112.

[23] Ming L F, Yue H, Xu L M, *et al.* Hydrothermal synthesis of oxidized g-C_3N_4 and its regulation of photocatalytic activity [J]. *J Mater Chem A*, 2014, **2**(45): 19145-19149.

[24] Huang H, Huang N, Wang Z H, *et al.* Room-temperature synthesis of carnation-like ZnO@AgI hierarchical nanostructures assembled by AgI nanoparticles-decorated ZnO nanosheets with enhanced visible light photocatalytic activity [J]. *J Coll Interf Sci*, 2017, **502**: 77-88.

[25] He L L, Tong Z F, Wang Z H, *et al.* Effects of calcination temperature and heating rate on the photocatalytic properties of ZnO prepared by pyrolysis [J]. *J Coll Interf Sci*, 2018, **509**: 448-456.

[26] Xu M, Han L, Dong S J. Facile large-scale synthesis of

urea-derived porous graphitic carbon nitride with extraordinary visible-light spectrum photodegradation [J]. *ACS Appl Mater Inter*, 2013, **5**(16): 12533-12540.

[27] Cui Y J, Zhang G G, Lin Z Z, *et al.* Condensed and low-defected graphitic carbon nitride with enhanced photocatalytic hydrogen evolution under visible light irradiation [J]. *Appl Catal B: Environ*, 2016, **181**: 413-419.

[28] Han Q, Wang B, Gao J, *et al.* Atomically thin mesoporous nanomesh of graphitic C(3)N(4) for high-efficiency photocatalytic hydrogen evolution [J]. *ACS nano*, 2016, **10**(2): 2745-2751.

[29] Song X P, Yang Q, Jiang X H, *et al.* Porous graphitic carbon nitride nanosheets prepared under self-producing atmosphere for highly improved photocatalytic activity [J]. *Appl Catal B: Environ*, 2017, **217**: 322-330.

[30] Xu G L, Zhang H B, Wei J, *et al.* Integrating the *g*-C_3N_4 nanosheet with B-H bonding decorated metal-organic framework for CO_2 activation and photoreduction [J]. *ACS nano*, 2018, **12** (6): 5333-5340.

[31] Sun C Z, Hui Z, Hao L, *et al.* Enhanced activity of visible-light photocatalytic H_2 evolution of sulfur-doped *g*-C_3N_4 photocatalyst via nanoparticle metal ni as cocatalyst [J]. *Appl Catal B: Environ*, 2018, **235**: 66-74.

[32] Zheng Y M, Li N, Zhang W D. Preparation of nanostructured microspheres of Zn-Mg-Al layered double hydroxides with high adsorption property [J]. *Coll* Surf *A Physicochem Eng Asp*, 2012, **415**: 195-201.

[33] Herrmann J M, Tahiri H, Guillard C, *et al.* Photocatalytic degradation of aqueous hydroxy-butandioic acid (malic acid) in contact with powdered and supported titania in water[J]. *Catal Today*, 1999, **54**: 131-141.

[34] Rong X S, Qiu F X, Rong J, *et al.* Synthesis of porous *g*-C_3N_4/La and enhanced photocatalytic activity for the degradation of phenol under visible light irradiation [J]. *J Sol State Chem*, 2015, **230**: 126-134.

[35] Liu G, Niu P, Yin L C, *et al.* α-Sulfur crystals as a visible-light-active photocatalyst [J]. *J Am Chem Soc*, 2012, **134**: 9070-9073.

EDTA 有效促进石墨相氮化碳(*g*-C_3N_4)光催化降解甲基橙

唐 丹, 尹梦云, 宋雪平, 周丽梅, 周娅芬*

(四川省化学合成与污染控制重点实验室, 西华师范大学 化学化工学院, 四川 南充 637002)

摘要: 研究了在光照下, 乙二胺四乙酸 (EDTA) 的添加促进石墨相氮化碳(*g*-C_3N_4)光催化降解甲基橙(MO). 研究了 H^+和羧酸根负离子对光降解 MO 的影响. 紫外-可见漫反射光谱 (DRS) 研究表明, EDTA 的加入并没有改变 *g*-C_3N_4的电子结构和光电特性. EDTA 的加入捕获了空穴(h^+), 促进了光生 e^-/h^+对的分离, 从而使光降解活性提高. 证明了 $\cdot O_2^-$是光催化降解过程中的主要活性物种. 基于上述研究结果, 我们提出了一种可能的 EDTA 促进 *g*-C_3N_4光催化降解 MO 的机理. 这些结果为提高 *g*-C_3N_4光催化降解水体中有机污染物的性能提供了一种新方法.

关键词: 石墨相氮化碳; 乙二胺四乙酸; 甲基橙; 光催化; 光降解